Photosensitized and photocatalyzed degradation of azo dye using Ln^{n+}-TiO_2 sol in aqueous solution under visible light irradiation

Yibing Xie [a, b], Chunwei Yuan [a], Xiangzhong Li [b]

[a] *Key Laboratory of Molecular & Biomolecular Electronics, Southeast University, Nanjing 210096, China*

[b] *Department of Civil and Structural Engineering, The Hong Kong Polytechnic University, Hong Kong*

Abstract

With attempts to improve the photocatalytic activity of titanium dioxide (TiO_2) catalysts and also extend the light absorption toward the visible light region, three types of the lanthanide ion-modified titanium dioxide (Ln^{n+}-TiO_2) sol catalysts were prepared by a chemical method of coprecipitation-peptization. The microstructure and morphology of Ln^{n+}-TiO_2 sol samples were characterized by atom force microscope, particle size distribution, and X-ray diffraction measurements. The analytical results showed that these sol catalysts had better particles distribution and interfacial adsorption ability than the powder catalysts in suspension. The photocatalytic degradation of azo dye (X-3B) in Ln^{n+}-TiO_2 hydrosol reaction system was studied to determine photocatalytic activity of the crystallized Ln^{n+}-TiO_2 sol catalysts. Both TiO_2 and Ln^{n+}-TiO_2 sol catalysts demonstrated higher photocatalytic reactivity than Deggusa P25 TO_2 powder catalyst significantly. The experiments also confirmed that the modification of TiO_2 with lanthanide ions doping can improve the efficiency of interfacial adsorption and photocatalytic reactivity with azo dye. The photocurrent response of catalysts under visible light irradiation showed that the Ln^{n+}-TiO_2 sol catalysts had significant absorption to visible light. Since this hydrosol reaction system using the Ln^{n+}-TiO_2 sol catalyst has several advantages over most conventional powder reaction systems, it may provide a new approach for further development of photocatalytic reaction systems in the future.

Keywords: Hydrosol; Lanthanide ion; Photocatalysis; Photocurrent; Photosensitization

1. Introduction

Titanium dioxide (TiO_2) has proven to be the most effective and suitable catalyst for photocatalytic reaction due to its economical, chemically stable, and insoluble properties [1-3]. So far, a variety of physical and chemical approaches have succeeded to synthesize anatase and rutile TiO_2 catalysts, including sputtering synthesis [4], flame pyrolysis [5], electrochemical deposition [6], chemical vapor deposition [7], precipitation [8], and sol-gel methods [9]. However, the physico-chemical properties of the synthesized TiO_2 particles are significantly affected by the precursor used and the preparation procedure applied. For example, in the sol-gel methods, the pretreatment of sol particles and thermal treatment of powder particles have been observed to affect the phase formation and morphology of product TiO_2 particles [10]. In these methods, high temperature above 450 °C in calcination is usually required to form regular crystal structure. However, in the meantime, the high temperature treatment can decline the surface area and also lose some surface hydroxyl groups of TiO_2 catalysts. Alternatively, a new method of chemical coprecipitation-peptization to synthesize the crystallized TiO_2 sol at low temperature of < 100 °C became attractive to further improve the photocatalytic activity of TiO_2 catalysts. Compared with most TiO_2 powders, theses TiO_2 sol catalysts have several advantages of: (1) finer particle size with more uniform distribution and better dispersion in water; (2) stronger interfacial adsorption ability; and (3) easy coating on different supporting materials including those substrates with a poor character of thermal resistance such as some polymers, optical fibers, plastics, wood, and papers. However, it is generally believed that most sol without high temperature treatment has an amorphous structure, which contains non-bridging oxygen in the bulk TiO_2 and a lot of Ti-O atomic arrangement defects acting as centers for recombination of photogenerated electron-hole pairs. Therefore, a regular crystal structure is the prerequisite for TiO_2 semiconductor acting as an effective photocatalyst [11]. Additionally, the crystal phase of TiO_2 is also a critical factor. The anatase phase usually showed a better photocatalytic activity than the rutile phase [12,13].

On the other hand, many studies have succeeded in addition of either metals or metallic oxides into TiO_2 structure to extend the light absorption toward the visible light range and also to eliminate the recombination of holes (h^+) and electrons (e^-). Some recent studies have been focused on the doping with lanthanide ions/oxides with 4*f* electron configuration because lanthanide ions could form complexes with various Lewis bases including organic acids, amines, aldehydes, alcohols, and thiols in the interaction of the functional groups with their *f*-orbital [14-16]. Xu et al. [14] reported that doping with La^{3+}, Ce^{3+}, Er^{3+}, Pr^{3+}, Gd^{3+}, Nd^{3+}, or Sm^{3+} was beneficial to NO_2^- adsorption. Ranjit and his co-workers [15,16] reported that doping with Eu^{3+}, Pr^{3+}, or Yb^{3+} increased the adsorption capacity and also adsorption rate of TiO_2 catalysts simultaneously in aqueous salicylic acid, *t*-cinnamic acid, and *p*-chlorophenoxy-acetic acid solutions. However, the effect of lanthanide oxides on the separation of electron-hole pairs and the photoresponse had not been extensively investigated so far. For all lanthanide ions, they have special electronic structure of $4f^x5d^y$ which would lead to different optical properties and dissimilar catalytic properties, and also have a redox couple of $Ln^{n+}/Ln^{(n+1)+}$ which would be able to form the labile oxygen vacancies (OV) with the relatively high mobility of bulk oxygen species [17].

In this study, three kinds of lanthanide ion-doped TiO_2 (Ln^{n+}-TiO_2) sol catalysts including Nd^{3+}-TiO_2, Eu^{3+}-TiO_2, and Ce^{4+}-TiO_2, and also a pure TiO_2 sol catalyst were prepared using a chemical method of coprecipitation-peptization at low temperature and ambient pressure. The photocatalytic activity of these sol samples was evaluated in photocatalytic degradation of azo dye (Reactive brilliant red – X-3B) in aqueous solution under visible light irradiation.

2. Experimental

2.1. Materials

TiO_2 powder (Degussa P25) with 80% anatase and 20% rutile was purchased from Degussa AG Company, which had a BET area of 50 $m^2\ g^{-1}$. Titanium tetrachloride

($TiCl_4$) chemical with reagent grade was obtained from J&K Chemical Ltd. Neodymium oxide (Nd_2O_3), europium oxide (Eu_2O_3), and cerium oxide (CeO_2) with purity of > 99.9% were purchased from Aldrich Chemical Co. Reactive brilliant red azo dye (X-3B) as a model chemical with reagent grade was obtained from Shanghai Dyestuff Chemical Plant and used without further purification. All other chemicals with analytical reagent grade were applied. Deionized and doubly distilled water was used throughout this study.

2.2. Preparation of Ln^{n+}-TiO_2 sol catalysts

The Ln^{n+}-TiO_2 sol samples were prepared by coprecipitation-peptization with the following procedure: lanthanide oxide (Nd_2O_3, Eu_2O_3, or CeO_2) was respectively dissolved into 100 mL of diluted hydrochloric acid solution with a proper amount up to 3.0% Ln^{n+} by atom fraction; 50 mL of titanium titrechloride ($TiCl_4$) was hydrolyzed and diluted with the above frozen acidic solution at temperature below 0 °C under vigorous stirring for 2 h; to ensure a complete hydrolysis, diluted aqueous ammonium (NH_4^+) solution (10 wt.%) was added dropwise into the transparent $TiCl_4$ solution to obtain colloid precipitate at pH 10; the residual NH_4^+ and Cl^- ions in the precipitate were removed by washing with water till the pH of filtrate dropped to 7.5; the purified Ln^{n+}-TiO_2 colloid suspension was continuously stirred at room temperature with addition of nitric acid as a peptization aid and also a phase-transfer accelerant till pH was further down to 1.5 to form the transparent Ln^{n+}-TiO_2 sol as primary rough sol; This rough sol was further peptized for 8 h at 25 °C with stirring, and then digested at 70 °C for 12 h in an air-free condition; eventually the product Ln^{n+}-TiO_2 regular sol was formed with uniform, stable, and transparent properties. These nano-sized sol particles can maintain a homogenous distribution for a quite long time. In addition, a TiO_2 sol sample was also prepared in the same procedure, but without doping with lanthanide ions.

2.3. Characterization of Ln^{3+}-TiO_2 sol catalysts

To determine the phase composition and crystal structure of the prepared sol

catalysts, X-ray diffraction (XRD) was carried out at room temperature using a X-ray diffractometer (Shimadazu XD-3A) with graphite monochromatic copper radiation (CuK_α, λ = 0.15418 nm), 40 kV as accelerating voltage, 40 mA as emission current. The particulate morphology of the sol catalysts was observed on atom force microscope (AFM, Nanoscope III System). The average particle size and particle size distribution (PSD) were determined by a light-scattering size analyzer (Zetasizer 3000HSA).

2.4. Photoreactor and Visible Light Source

A cylindrical quartz photoreactor with effective volume of 50 mL was used in this study as illustrated in Fig. 1. A 150-W halogen tungsten lamp with the average radiation intensity of 48.9 mW cm^{-2} and main emission in the range of 400-800 nm was used together with the UV and IR cut-off filters as a visible light source.

[Fig. 1]

The photocatalytic activity of the prepared TiO_2 and Ln^{n+}-TiO_2 sol catalysts was investigated in the photocatalytic degradation of reactive brilliant red azo dye (X-3B) in aqueous solution, while Degussa P25 TiO_2 powder catalyst was also used for comparison. The X-3B azo dye has a main absorption spectrum at 512-540 nm in the visible light range and its molecular structure is illustrated in Fig. 2.

[Fig. 2]

A set of X-3B adsorption isotherm experiments was carried out with the following procedure: the Ln^{n+}-TiO_2 sol or P25 TiO_2 powder catalyst with a designated amount of 2-20 mg was added into 10 mL of X-3B solution with an initial concentration of 100 mg L^{-1}; this aqueous mixture was kept at 25 °C and stirred for 120 min in the dark; then the mixture was centrifuged at 10,000 rpm for 15 min and then filtered by a 0.22-μm Millipore filter; the concentration of remaining X-3B in the mixture samples

after filtration was determined by a UV-VIS spectrometer (Shimadazu UV-2201).

A set of photocatalytic degradation experiments in aqueous X-3B solution was performed with the following procedure: 20 mg of sol catalyst was added into 20 mL of X-3B solution with an initial concentration of 100 mg L^{-1}; prior to photoreaction, the aqueous mixture was magnetically stirred in the dark for 30 min to reach adsorption-desorption equilibrium; then the reaction mixture with stirring was irradiated by the visible light from the top vertically; during the photoreaction, samples were collected at a time interval of every 15 min and then filtered by the 0.22-μm Millipore filter for UV-VIS spectrum analysis to determine the concentration of X-3B.

To determine the photo-response of such a hydrosol system under visible light irradiation, a set of experiments to measure photocurrent-time spectra was conducted in a standard three-electrode reactor system, which consists of a cell with a quartz side window, a saturated calomel reference electrode (SCE), a platinum plate counter-electrode (CE), and a indium-tin oxide (ITO) glass plate working electrode (WE). The aqueous solution containing 1.0 g L^{-1} Ln^{n+}-TiO_2 sol and 100 mg L^{-1} X-3B with an initial pH 3.5 was placed in the cell and the working electrode was dipped into the solution. After 30 min, Ln^{n+}-TiO_2 sol and X-3B dye in the solution were gradually adsorbed on the surface of the working electrode. Then the visible light was turned on in front of the working electrode and the photocurrent-time (I–t) profile was recorded with the CHI660 electrochemical workstation.

3. Results and discussion

3.1. XRD analysis

To determine the crystal structure and composition, the prepared TiO_2 and Ln^{n+}-TiO_2 sol samples were examined by XRD and the XRD patterns of different sol catalysts are shown in Fig. 3. It can be noted that the rough TiO_2 sol sample (Curve e) did not have any significant diffraction peaks representing the characteristic of

crystalline, which means it had a predominant amorphous structure. Although the nearly linear or branched oligomers (-Ti-O-Ti-O-) had been almost formed from the $TiCl_4$ precursor through the hydrolysis, precipitation, and neutralization pretreatment, a complete condensation-polymerization process still had not been achieved to let $Ti(OH)_4$ and $TiO(OH)_2$ form regular edge-sharing TiO_6 octahedra with long-range order inorganic network structure of in the bulk TiO_2. However, the XRD patterns of the regular TiO_2 and Ln^{n+}-TiO_2 sol samples showed several peaks at 2θ = 25.4º, 38.0º, 47.8º, 54.6º, 63.2º, 68.8º, 75.3º, and 82.8º which represented the formation of anatase structure. It seems that during the peptizing process, $TiOCl_2 \cdot nH_2O$ was readily hydrolyzed and the regular Ti-O-Ti bond from non-bridging oxygen in the bulk TiO_2 was almost completed by the polycondensation process. These results confirmed that the protonation of amorphous TiO_2 sol in inorganic strong acid medium with hot-water treatment could induce the TiO_2 crystallization process at befitting temperature of 70 °C and pH 1.5 to successfully achieve the phase transformation from amorphous to anatase, which commonly requires high temperature above 450 °C through calcination. Moreover, the Ln^{n+}-TiO_2 sol samples also showed several scattering peaks in the XRD patterns, which could be considered as the coexistence of somewhat semicrystalline structure in the bulk Ln^{n+}-TiO_2. The crystalline size of the prepared catalyst samples was calculated by using Scherrer's formula and determined to be 3.77 nm for Nd^{3+}-TiO_2, 4.30 nm for Eu^{3+}-TiO_2, 2.74 nm for Ce^{4+}-TiO_2 and 4.58 nm for TiO_2, respectively. Additionally, it can be found that all Ln^{n+}-TiO_2 sol samples showed broader diffraction peaks than the pure TiO_2 sol sample due to smaller grain sizes. It is also found that no diffraction peaks for any new crystal phase other than the anatase structure appeared in the XRD patterns of Nd^{3+}-TiO_2, Eu^{3+}-TiO_2, and Ce^{4+}-TiO_2 sol samples. Since the radius of three lanthanide ions ($r(Nd^{3+})$ = 0.995Å, $r(Eu^{3+})$ = 0.947Å $r(Ce^{4+})$ = 1.01Å) are larger than that of titanium ion ($r(Ti^{4+})$ = 0.68Å). Under such a moderate temperature condition, the lanthanide ions would impossibly enter into the lattice structure of TiO_2 to replace Ti^{4+} ion. On the contrary, on the interface of Ln^{n+}-TiO_2, Ti^{4+} ion might substitute for lanthanide ions in the lattice of lanthanide oxides and a Ti-O-Ln bond could be formed. Shah et al. [18]

proposed that Nd^{3+} resides in the octahedral interstitial site for Nd^{3+}-TiO_2 and the high oxygen affinities of interstitially locating neodymium ion effectively create a localized positive charge around Ti or form an oxygen vacancy. In this study, the result of only anatase crystalline structure for Ln^{n+}-TiO_2 catalyst means that the phase behavior of the doping lanthanide oxide is either an amorphous structure or an interstitial solid solution between interconnecting TiO_6 octahedrons.

[Fig. 3]

3.2. AFM analysis

To determine the morphology of catalysts, Ln^{n+}-TiO_2 sol and P25 TiO_2 powder catalysts were observed by AFM and their images are shown in Fig. 4. It can be seen that TiO_2 sol particles appeared a spherical shape and had an average particle size of about 25 nm. It was observed that these TiO_2 sol particles were uniformly distributed and no agglomeration was observed. Compared with the sol samples, P25 TiO_2 powder particles were significantly bigger with a particle size of about 45 nm and aggregated size of about hundreds nanometer. The AFM results showed that TiO_2 sol had no significant aggregation and better dispersion in its colloid solution than P25 TiO_2 powder. Furthermore, three types of Ln^{n+}-TiO_2 sol catalysts had a similar spherical shape with smaller particle sizes of about 10 nm, 8 nm, and 12 nm for Nd^{3+}-TiO_2, Eu^{3+}-TiO_2 and Ce^{4+}-TiO_2, respectively. These results indicated that lanthanide ion doping could hinder the aggregation and growth of sol particles, which resulted in the decrease in grain sizes and the increase in the specific surface areas.

[Fig. 4]

3.3. PSD analysis

Due to interaction between sol particles in the aqueous dispersion medium, these particles seldom have a uniform size and normally vary in a certain range [19,20]. The particle size distribution of catalysts greatly influences their properties of adsorption

and photoactivity. In this study, the particle size of TiO_2 and Ln^{3+}-TiO_2 catalysts was analyzed by the light-scatting size analyzer and the particle size distribution of different catalysts is presented in Fig. 5. The results demonstrated that P25 TiO_2 powder had a PSD in the range 148-208 nm with a mean value of 174 nm in its aqueous suspension and the pure TiO_2 sol had a PSD in the range of 13.8-35.3 nm with a mean value of 21.1 nm. These results indicated that all the sol catalysts were much smaller in size and had a single-modal distribution characteristic with more uniform PSD than the P25 TiO_2 powder catalyst. Furthermore, the results showed that Nd^{3+}-TiO_2 sol had an average size of 8.5 nm and PSD from 4.6 to 16.4 nm; Eu^{3+}-TiO_2 sol had an average size of 3.5 nm and PSD from 3.5 to 17.2 nm; and Ce^{4+}-TiO_2 sol had an average size of 10.5 nm and PSD from 8.5 to 18.6 nm. These data confirmed that the particle size of TiO_2 sol was further reduced by doping with lanthanide ions significantly. Therefore, above experimental results indicated that the modification by lanthanide ions would be beneficial to stabilize the nano-sized Ln^{n+}-TiO_2 sol particles in aqueous solution with a good dispersion nature. These PSD results of TiO_2 and Ln^{n+}-TiO_2 sol samples were in good agreement to the results by the AFM measurement.

[Fig. 5]

3.4. X-3B adsorption isotherm

Since the heterogeneous photocatalytic reaction mainly occurrs at the interface of substrate and photocatalyst, the interfacial adsorption effect and affinity property play important roles in an overall reaction rate [21,22]. The effect of adsorption-desorption equilibrium was investigated between X-3B and different catalysts in aqueous solution under darkness.

On the basis of experimental data, X-3B adsorption isotherms on the different Ln^{n+}-TiO_2 catalysts were calculated using the Langmuir adsorption model as Equation 1.

$$\frac{C_e}{\Gamma} = \frac{1}{\Gamma_{max}} \cdot C_e + \frac{1}{K_a \cdot \Gamma_{max}} \quad (1)$$

where C_e is the equilibrium concentration of the substrate in the solution in mol L^{-1}, K_a is the adsorption equilibrium constant in L mol^{-1}, and Γ_{max} is the saturated adsorption amount in mol g^{-1}.

The experimental results are expressed by plotting C_e/Γ_{ads} versus C_e in Fig. 6. It can be seen that the adsorption data were well fitted by the Langumiur model in its linear form. The saturation adsorption capacity was determined from high to low as 0.0606 mmol g^{-1} for Eu^{3+}-TiO_2 > 0.0579 mmol g^{-1} for Nd^{3+}-TiO_2 > 0.0500 mmol g^{-1} for Ce^{4+}-TiO_2 > 0.0413 mmol g^{-1} for TiO_2 > 0.0345 mmol g^{-1} for P25 TiO_2. These results indicated that all the Ln^{n+}-TiO_2 sol catalysts exhibited higher adsorption capacity than both the TiO_2 sol and P25 TiO_2 powder. Since the Ln^{n+}-TiO_2 sol had finer particle size, larger special surface area and much better dispersion in aqueous solution than the TiO_2 sample, these factors would result in better adsorption ability physically. Furthermore, the lanthanide ions of Ln^{n+}-TiO_2 sol particle could form the O-Ln-O-Ti-O structure by chemical bonding with oxygen ions [15], while X-3B dye molecule is negatively charged due to the $–SO_3Na$ group in its chemical structure. In this case, the Ln^{n+} ions could act as Lewis acid because of their partial unoccupied 4*f* atomic orbits and X-3B dye could act as Lewis base due to its π electron conjugation structure. Consequently the formation of a Lewis acid-base complex of $RSO_3^{-}\cdots Ln^{n+}$-TiO_2 between lanthanide ion and X-3B dye in aqueous solution could enhance the interface adsorption chemically as well [23].

[Fig. 6]

3.5. Photocatalytic degradation of X-3B under visible light irradiation

To evaluate the photocatalytic activity of Ln^{n+}-TiO_2 catalysts, several experiments of X-3B degradation were carried out in either aqueous solution or suspension with

the initial X-3B concentration of 100 mg L^{-1} and catalysts dosage of 1.0 g L^{-1}. Each experiment lasted for 120 min and samples were collected every 15 min for analysis to determine X-3B concentration by the UV-VIS spectroscopy. The experimental results are shown in Fig. 7. The results showed that X-3B concentration decreased under visible illumination remarkably. The Langmuir-Hinshelwood (L-H) kinetic equation was one of the most useful models to describe this type of reaction. However, in this study, the $K_{ads}C_0$ values in the adsorption tests were determined to be 0.1119 for P25 TiO_2 powder, 0.1715 for TiO_2 sol, 0.2179 for Ce^{4+}-TiO_2 sol, 0.2792 for Eu^{3+}-TiO_2, 0.2642 for Nd^{3+}-TiO_2, respectively. Since these $K_{ads}C$ values were much lower than 1, the L-H model can be simplified into the first-order model**.** The experimental data were well fitted by the first-order model and the kinetic constant k of X-3B degradation using different catalysts are presented in Table 1. The experimental results indicated that the reaction rates with different catalysts from high to low were ranked as Nd^{3+}-TiO_2 sol > Eu^{3+}-TiO_2 sol > Ce^{4+}-TiO_2 sol > TiO_2 sol > P25 TiO_2 powder. These results confirmed that all the sol catalysts performed faster degradation rates than the powder catalyst and all the Ln^{n+}-TiO_2 sol catalysts performed better than the pure TiO_2 sol. Among them, Nd^{3+}-TiO_2 sol catalyst achieved the highest X-3B degradation rate.

[Fig. 7]

[Table 1]

Since X-3B dye is a photosensitizer under visible illumination, the direct photolysis and photosensitized oxidation should be considered in this dye-Ln^{n+}-TiO_2 hydrosol system. The X-3B dye could be oxidized by the singlet oxygen ($^1O_2^*(S_1)$), which is generated from ground state oxygen ($^3O_2$) by absorbing photon energy emitted from the excited triplet state of dye molecule ($^3Dye^*(T_1)$). However, the experimental result shown in Fig. 7 confirmed that the direct photolysis of X-3B under visible illumination for 120 min was only achieved by about 1.4%. It means

that the direct photolysis was an insignificant factor due to low electron or energy transfer efficiency between the molecule complex ($O_2 \cdots$Dye).

It is generally believed that the TiO_2/UV photocatalytic oxidation in aqueous solution highly depends on (1) the generation efficiency of electron-hole from catalysts under illumination, (2) the separation efficiency of photogenerated electrons, and (3) the transfer efficiency of electrons and holes to surrounding supports or compounds adsorbed on the catalyst surface. However, the mechanism of photoreaction in such a Dye/TiO_2/Visible light system is actually more complicated than that in a TiO_2/UV light system.

3.6. Photoelectron generation under visible light illumination

To study the generation of photoelectrons in the X-3B/Ln^{n+}-TiO_2/Vis light hydrosol system, three sets of experiments were carried out to measure the photocurrent response of X-3B dye and Ln^{n+}-TiO_2 catalysts under visible light illumination in an on-off cycle mode. The first set of photocurrent experiments was conducted using P25 TiO_2 powder and pure TiO_2 sol, respectively in the aqueous solution with and without X-3B, and the results are shown in Fig. 8. The results showed that no significant photocurrent response occurred in both the P25 TiO_2 powder suspension and pure TiO_2 sol solution without X-3B dye, while visible light was either on or off. However, when X-3B dye existed in aqueous solution, it can be seen clearly that the photocurrent upsurge and dropping off occurred, while visible light was on and off in two cycles. The photocurrent intensity quickly increased to 0.352 μA in the X-3B /P25 TiO_2 powder suspension and to 0.495 μA in the X-3B/TiO_2 sol solution, respectively. These results confirmed that photoelectrons were generated under visible light illumination by X-3B dye, but not the TiO_2 catalysts. Under visible light illumination, the X-3B dye was exited from its ground singlet state to the excited triplet state. Then X-3B dye injected its excited electrons into the conduction band of TiO_2 to generate photoelectrons in the system.

[Fig. 8]

The second set of photocurrent experiments was carried out using three Ln^{3+}-TiO_2 catalysts in aqueous solution without X-3B dye and the experimental results are shown in Fig. 9. The results showed that the photocurrent was maintained at almost 0 during the initial period in the dark and rapidly increased to 0.265 μA for Nd^{3+}-TiO_2, 0.122 μA for Eu^{3+}-TiO_2 and 0.245 μA for Ce^{4+}-TiO_2, respectively, once light was on. In the meantime, it was also found that the photocurrent dropped off sharply to about 0.02 μA, while light was off. These results confirmed that the photoelectrons were successfully generated under visible light illumination by the Ln^{3+}-TiO_2 catalysts. Comparing the results of two sets of experiments, it can be indicated that X-3B was more sensitive than the Ln^{3+}-TiO_2 catalysts to generate photocurrent under visible light illumination. Since lanthanide metals have partially-filled atomic *d* or *f* shell, the electrons at Ln^{n+} 4*f* orbit could conduct electron-excitation and electron-transition to build up lanthanide ions with a higher valence state by absorbing proper photons energy. Consequently, surrounding Ln^{n+} ions may mutually bond due to self-sensitization and form positively-charged lanthanide ions cluster $(Ln_p)^{q+}$ ($q>3p$). This lanthanide cluster had discrete empty multi-energy levels below the conduction band of crystalline TiO_2. Their presence allowed a new electronic transition from the TiO_2 valence band to the empty lanthanide ion cluster energy levels known as a sub-band gap with less energy than TiO_2 valence-conduction band transition [24].

[Fig. 9]

The third set of photocurrent experiments was carried out in the X-3B/Ln^{n+}-TiO_2 solution under visible light illumination and the experimental results are shown in Fig. 10. The results demonstrated that photocurrent intensity was generated up to higher levels of 0.565 μA for X-3B/Eu^{3+}-TiO_2, 0.634 μA for X-3B/Nd^{3+}-TiO_2, and 0.816 μA for X-3B/Ce^{4+}-TiO_2, respectively during the instant illumination time. Once light was off, photocurrent quickly dropped off to 0.074 μA for X-3B/Eu^{3+}-TiO_2, 0.092 μA for

X-3B/Nd^{3+}-TiO_2 and 0.062 μA for X-3B/Ce^{4+}-TiO_2, respectively. The experimental results indicated that the photocurrent generation in the X-3B/Ln^{n+}-TiO_2 system was significantly stronger than that in either Ln^{n+}-TiO_2 only or X-3B only. Furthermore, the experimental results demonstrated two different patterns of photocurrent-time profiles. In the X-3B/Nd^{3+}-TiO_2 and X-3B/Ce^{4+}-TiO_2 hydrosol systems, once light was on, the photocurrent rapidly increased to 0.634 μA for Nd^{3+}-TiO_2 and 0.816 μA for Ce^{4+}-TiO_2, respectively and well maintained within instant illumination time. Once light was off, their current quickly dropped off to 0.092 μA for Nd^{3+}-TiO_2 and 0.062 μA for Ce^{4+}-TiO_2, respectively. However, in the Eu^{3+}-TiO_2 hydrosol system, the photocurrent instantly increased as well once light was on and further increased to a peak value of 0.565 μA after 20 seconds gradually. Once light was off, it decreased to the initial value of 0.074 μA, but not as quickly as those in the X-3B/Ce^{4+}-TiO_2 and X-3B/Nd^{3+}-TiO_2 systems. Additionally, the higher photocurrent generation indicated excellent light absorption ability of the X-3B/Ln^{n+}-TiO_2 system.

[Fig. 10]

3.7. Efficiency of photoelectron trapping and transferring

On the other hand, the lanthanide ions bonded on the surface of TiO_2 particles could act as good scavengers to trap photoelectrons, resulting in depressing photocurrent generation. As an overall result, only a small amount of electrons photogenerated can transfer to the working electrode to form an out-circuit. Comparing the photocurrent generation in three systems under the same experimental condition, the higher photocurrent intensity occurred in the X-3B/Ce^{4+}-TiO_2 solution might indicate that cerium ion had weaker electron-trapping capacity, while the lower photocurrent intensity occurred in the X-3B/Eu^{3+}-TiO_2 solution pointed out that europium ion had stronger electron-trapping capacity. According to the standard redox potentials of $E^0(O_2/O_2^-)$ = +0.338 V, $E^0(Nd^{3+}/Nd^{2+})$ = -0.40 V, $E^0(Eu^{3+}/Eu^{2+})$ = -0.35 V, $E^0(Ce^{4+}/Ce^{3+})$ = +1.76 V, and $E_{vb}(TiO_2)$ = -0.5 V versus NHE, the presence of Nd^{3+} and Eu^{3+} ion on the TiO_2 surface may promote the following reactions:

Step 1: $dye^{*} + CB(TiO_2) \rightarrow dye^{+} + e\text{-}CB(TiO_2)$ (electron injection)

Step 2: $Eu^{3+} + e \rightarrow Eu^{2+}$ or $Nd^{3+} + e \rightarrow Nd^{2+}$ (electron trapping)

Step 3: $Eu^{2+} + O_2 \rightarrow Eu^{3+} + O_2^{-}$ or $Nd^{2+} + O_2 \rightarrow Nd^{3+} + O_2^{-}$ (electron transferring)

However, cerium ion can only undergo electronic trapping (Step 2) of $Ce^{4+} + e \rightarrow Ce^{3+}$, but the reversed reaction with oxygen from Ce^{3+} to Ce^{4+} to achieve electron transferring (Step 3) is forbidden due to its higher redox potential than that of O_2/O_2^{-}. Consequently, its catalytic efficiency gradually declined because of the suppression of further recovery electron transfer. Therefore, Eu^{3+}-TiO_2 and Nd^{3+}-TiO_2 catalysts demonstrated better photocatalytic activity than Ce^{4+}-TiO_2 catalyst for X-3B degradation under visible light irradiation. It is a good agreement between the results of photocatalytic degradation experiments and photocurrent response experiments.

3.8. Mechanism of photosensitization of X-3B/Ln^{n+}-TiO_2 under visible light illumination

It is generally believed that pure TiO_2 can not be directly excited by visible light due to its high band-gap of 3.2 eV. The X-3B/Ln^{3+}-TiO_2 under visible light illumination has an entirely different mechanism of photo-excitation from TiO_2 under UV irradiation. The X-3B dye sensitization process involves the excitation of dye molecules by absorbing visible light photons and subsequent electron injection from excitation state dye to TiO_2 conduction band (CB). Then electrons underwent transfer process from CB to the working electrode (ITO conductive film) and finally formed out-circuit. In such a Dye/Ln^{n+}-TiO_2/Vis hydrosol system, Ln^{n+}-TiO_2 particles act as a bridge-band connecting X-3B dye and working electrode. Some key reactions are proposed in Equations 2-7.

$$Dye + h\nu \rightarrow Dye^{*} \quad (2)$$

$$Dye^{*} + TiO_2 \rightarrow TiO_2(e^{-}) + Dye^{+\cdot} \quad (3)$$

$$TiO_2(e^{-}) + O_2 \rightarrow O_2^{-\cdot} + TiO_2 \quad (4)$$

$$Ln^{n+} + TiO_2(e^{-}) \rightarrow Ln^{(n-1)+} + TiO_2 \quad (5)$$

$$Ln^{(n-1)+} + O_2 \rightarrow O_2^{-} + Ln^{n+} \quad (6)$$

$$O_2^{-\cdot} + Dye^{+\cdot} \rightarrow \text{Intermediates or final products} \quad (7)$$

In the above reactions, dye can be excited under visible light illumination (Equation 2). The excited state dye molecule can inject electrons into the conduction band of TiO_2 (Equation 3) and may be trapped by the electron scavengers of usually surrounding oxygen molecule (Equation 4). In the meantime, it is also extremely susceptible for the recombination between cationic radicals and the electrons if the injection electrons accumulate in the CB of TiO_2. So, the electrons trapping (Equation 5) and electrons transferring (Equation 6) become two key steps to inhibit electron-cationic radical recombination. The cationic radical ($dye^{+\cdot}$) produced by electron injection is less stable than the probe molecule in ground state dye. As a result, unstable dye cationic radicals can be directly degraded into its products by reacting with super-oxidizing anionic radials or other active oxygen (HO·, HOO· and $O_2^{-\cdot}$) (Equation 7). In particular, the lanthanide ion doped in TiO_2 plays an important role in promoting the electron trapping and electron transferring significantly in the Dye/Ln^{3+}-TiO_2 hydrosol system. The photosensitization reaction mechanism and potential states in the Dye/Ln^{n+}-TiO_2/Vis system are further illustrated in Figs. 11 and 12, respectively.

[Fig. 11]

[Fig. 12]

4. Conclusion

TiO_2 sol particles with 3.0 at.% lanthanide ion modification was prepared using chemical coprecipitation-peptization route. Ln^{n+}-TiO_2 sol particles showed regular crystal structure and narrow particle size distribution. Direct conversion from amorphous to nanocrystalline phase was achieved at moderate temperature of 70 °C and strong acidic condition of pH 1.5. The Ln^{n+}-TiO_2 sol exhibited better interfacial adsorption effects under the dark condition and higher photocatalytic activity under visible light irradiation than pure TiO_2 sol and P25 TiO_2 powder. Concerning the

photocurrent response in X-3B/Ln^{n+}-TiO_2/Vis hydrosol system, Nd^{3+}-TiO_2 and Eu^{3+}-TiO_2 showed weaker photoelectrons generation than Ce^{4+}-TiO_2, probably due to the difference of electron-scavenging capability by different lanthanide ions. In terms of X-3B degradation efficiency, Nd^{3+}-TiO_2 and Eu^{3+}-TiO_2 showed higher photocatalytic activity than Ce^{4+}-TiO_2, which might result from the difference of standard redox potentials of $Ln^{n+}/Ln^{(n-1)+}$ ion pairs.

Acknowledgements

This work was financially supported by the Hi-Tech Research and Development Program (863 Program) of China (Grant No. 2002AA302304), the National Natural Science Foundation of China (Grant No. 60121101) and also the Research Grants Council of Hong Kong (Grant No. PolyU5148/03E).

References

[1] A. Fujishima, T.N. Rao, D.A. Tryk, J. Photochem. Photobiol. C: Rev. 1 (2001) 1.

[2] J.M. Herrmann, Catal. Today 53 (1999) 11.

[3] S. Malato, J. Blanco, A Vidal, D. Alarcon, M.I. Maldonado, J. Caceres, W. Gernjak, Solar Energy 75 (2003) 329.

[4] D. Mardare, M. Tasca, M. Delibas, G.I. Rusu, Appl. Surf. Sci. 156 (2000) 200.

[5] S.U.M. Khan, M. Al-Shahry, W.B. Ingler Jr, Science 297 (2002) 2243.

[6] G.M.Wang, H. Chen, H. Zhang, C.W. Yuan, Z.H. Lu, G.M. Wang, W.Y. Yang, Appl. Surf. Sci. 135 (1998) 97.

[7] D.H. Kuo, C.N. Shueh, Chem. Vap. Deposition 9 (2003) 265.

[8] T. Kawahara, T. Ozawa, M. Iwasaki, H. Tada, S. Ito, J. Colloid Interf. Sci. 267 (2003) 377.

[9] N.I. Al-Salim, S.A. Bagshaw, A. Bittar, T. Kemmitt, A.J. McQuillan, A.M. Mills, M.J. Ryan, J. Mater. Chem. 10 (2000) 2358.

[10] S.S. Watson, D. Beydoun, J.A. Scott, R. Amal, Chem. Eng. J. 95 (2003) 213.

[11] H.K. Park, D.K. Kim, C.H. Kim, J. Am. Ceram. Soc. 80 (1997) 743.

[12] D. Švadlák, J. Shánélová, J. Málek, L.A. Pérez-Maqueda, J.M. Criado, T.

Mitsuhashi, Thermochim. Acta 414 (2004) 137.

[13] M. Koelsch, S. Cassaignon, C. Ta Thanh Minh, J.F. Guillemoles, J.P. Jolivet, Thin Solid Films 86-92 (2004) 451.

[14] W. Xu, Y. Gao, H.Q. Liu, J. Catal. 207 (2002) 151.

[15] K.T. Ranjit, I. Willner, S.H. Bossmann, A.M. Braun, J. Catal. 204 (2001) 305.

[16] K.T. Ranjit, I. Willner, S.H. Bossmann, A.M. Braun, Environ. Sci. Technol. 35 (2001) 1544.

[17] B.M. Reddy, P.M. Sreekanth, E.P. Reddy, Y. Yamada, Q. Xu, H. Sakurai, T. Kobayashi, J. Phys. Chem. B 106 (2002) 5695.

[18] S.I. Shah, W. Li, C.P. Huang, O. Jung, C. Ni, PNAS. 99 (2002), 6482-6486.

[19] E. Reverchon, P.G. Della, D. Sannino, P. Ciambelli, Powder Technol. 102 (1999) 127.

[20] A.A. Gribb, J.F. Banfield, Am. Mineral. 82 (1997) 717.

[21] P. Davit, G. Martra, S. Coluccia, V. Augugliaro, E. Garcia López, V. Loddo, G. Marci, L. Palmisano, M. Schiavello, J. Mol. Cataly. A: Chem. 204–205 (2003) 693.

[22] F.Y. Oliva, L.B. Avalle, O.R. Cámara, C.P. De Pauli, J Colloid Interf. Sci. 261 (2003) 299.

[23] K.T. Ranjit, H. Cohen, I. Willner, S.H. Bossmann, A.M. Braun, J. Mater Sci. 34 (1999) 5273.

[24] Y.B. Xie, C.W. Yuan, Appl. Surf. Sci. 221 (2004) 17.

Table 1 Kinetic parameters of X-3B photodegradation under visible light irradiation

Photocatalyst	k_{ap} (min^{-1})	$t_{1/2}$ (min)	r (%)	R
P25	0.00554	125.3	59.76	0.9977
TiO_2 sol	0.00667	103.9	67.92	0.9972
Nd^{3+}-TiO_2 sol	0.01499	46.2	89.14	0.9973
Eu^{3+}-TiO_2 sol	0.01246	55.6	85.25	0.9978
Ce^{4+}-TiO_2 sol	0.00729	95.1	72.39	0.9905

k_{ap}−apparent rate constant (min^{-1}); $t_{1/2}$−Half-Life (min); r−X-3B photodegradation ratio (%); R−correlation coefficient

List of Figure Captions

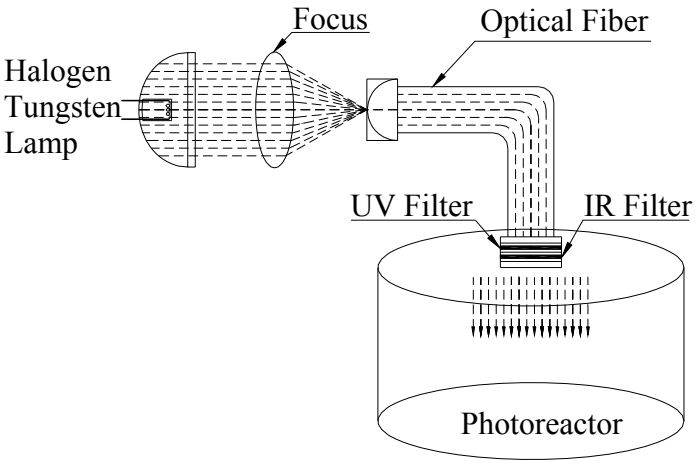
Focus
Optical Fiber
Halogen
Tungsten
Lamp
UV Filter
IR Filter
Photoreactor

Fig. 1.

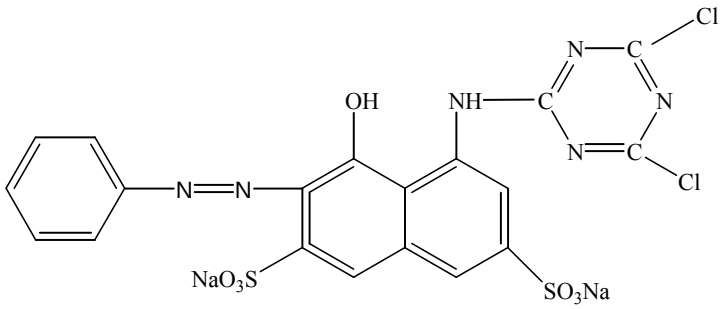

Fig. 2.

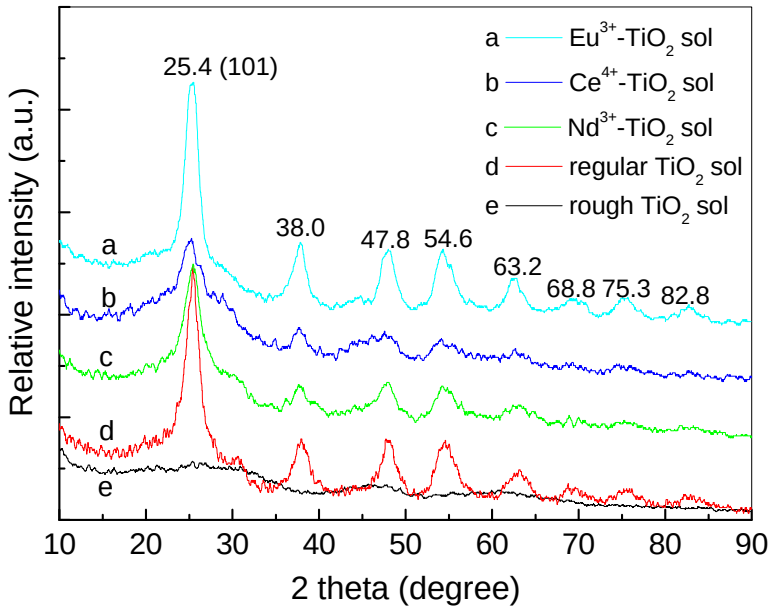
25.4 (101)
38.0
47.8
54.6
63.2
68.8
75.3
82.8
a
b
c
d
e
a Eu3+-TiO2 sol
b Ce4+-TiO2 sol
c Nd3+-TiO2 sol
d regular TiO2 sol
e rough TiO2 sol
Relative intensity (a.u.)
2 theta (degree)
10
20
30
40
50
60
70
80
90

Fig. 3.

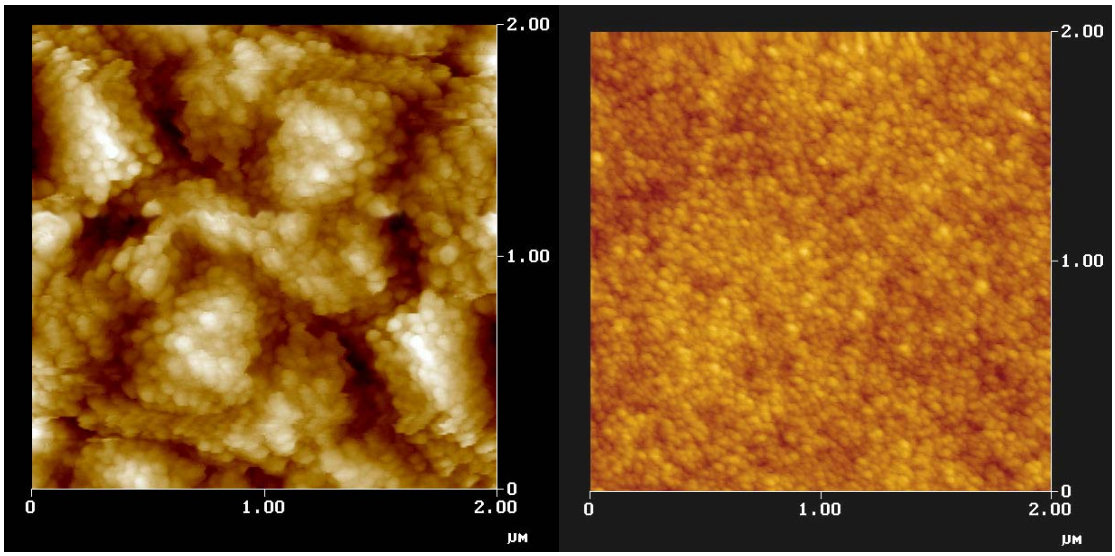

Fig. 4.

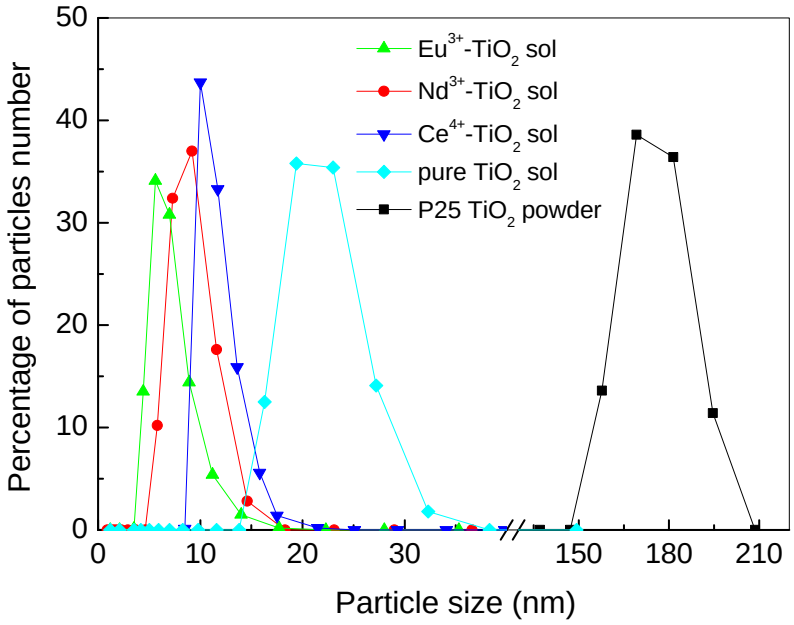
Percentage of particles number
Particle size (nm)
Eu3+-TiO2 sol
Nd3+-TiO2 sol
Ce4+-TiO2 sol
pure TiO2 sol
P25 TiO2 powder
0
10
20
30
40
50
0
10
20
30
150
180
210

Fig. 5.

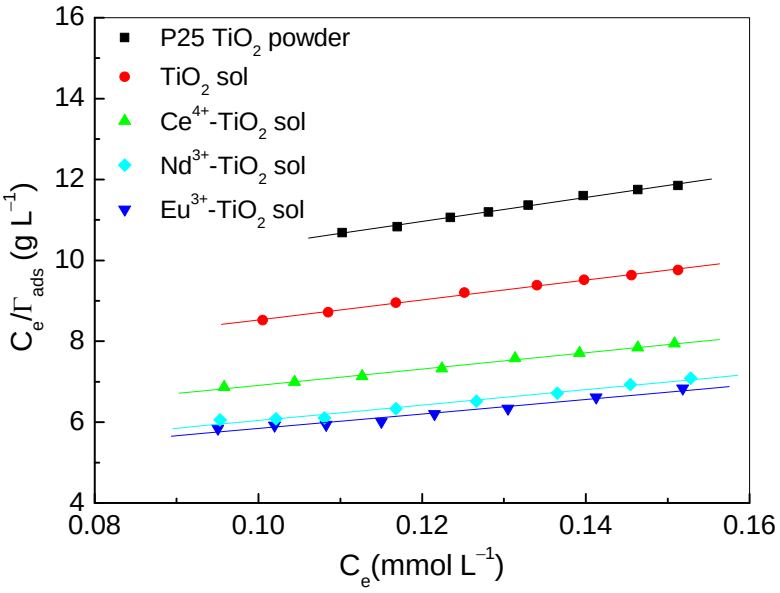
P25 TiO2 powder
TiO2 sol
Ce4+-TiO2 sol
Nd3+-TiO2 sol
Eu3+-TiO2 sol
Ce/Γads (g L−1)
Ce(mmol L−1)
16
14
12
10
8
6
4
0.08
0.10
0.12
0.14
0.16

Fig. 6.

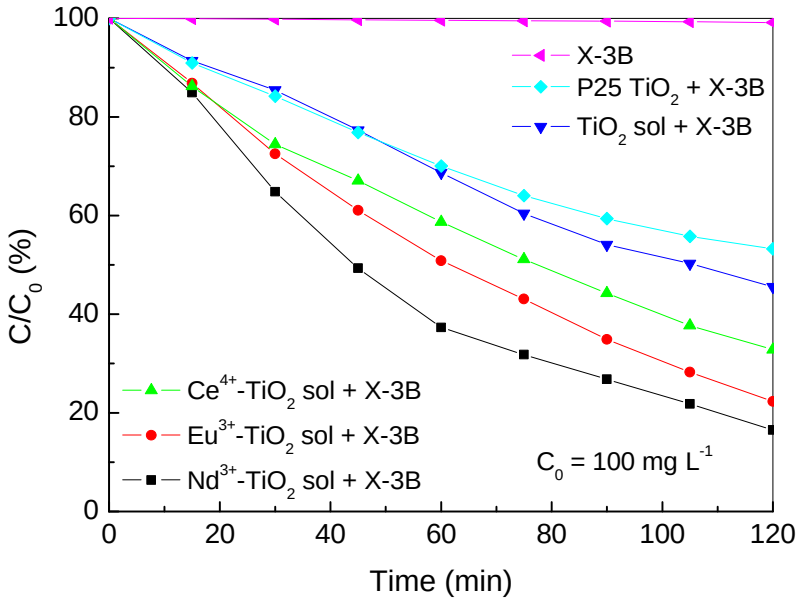
100
80
60
40
20
0
0
20
40
60
80
100
120
C/C0 (%)
Time (min)
X-3B
P25 TiO2 + X-3B
TiO2 sol + X-3B
Ce4+-TiO2 sol + X-3B
Eu3+-TiO2 sol + X-3B
Nd3+-TiO2 sol + X-3B
C0 = 100 mg L-1

Fig. 7.

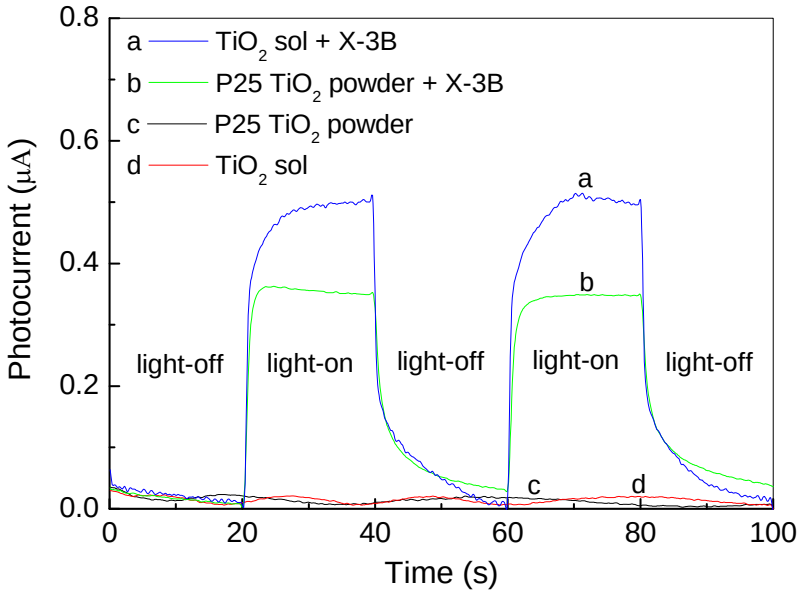
a TiO2 sol + X-3B
b P25 TiO2 powder + X-3B
c P25 TiO2 powder
d TiO2 sol
Photocurrent (μA)
Time (s)
light-off
light-on
light-off
light-on
light-off
a
b
c
d
0.0
0.2
0.4
0.6
0.8
0
20
40
60
80
100

Fig. 8.

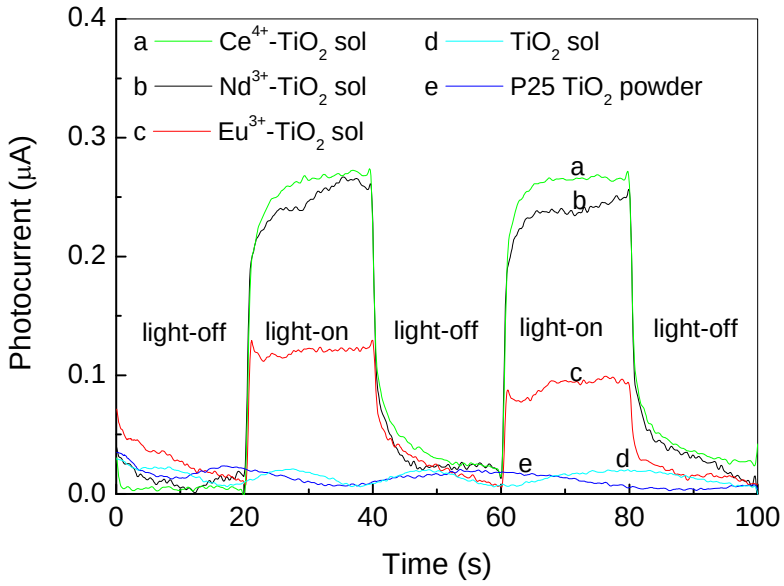
a Ce4+-TiO2 sol
b Nd3+-TiO2 sol
c Eu3+-TiO2 sol
d TiO2 sol
e P25 TiO2 powder
Photocurrent (μA)
Time (s)
light-off
light-on
light-off
light-on
light-off
a
b
c
d
e
0.0
0.1
0.2
0.3
0.4
0
20
40
60
80
100

Fig. 9.

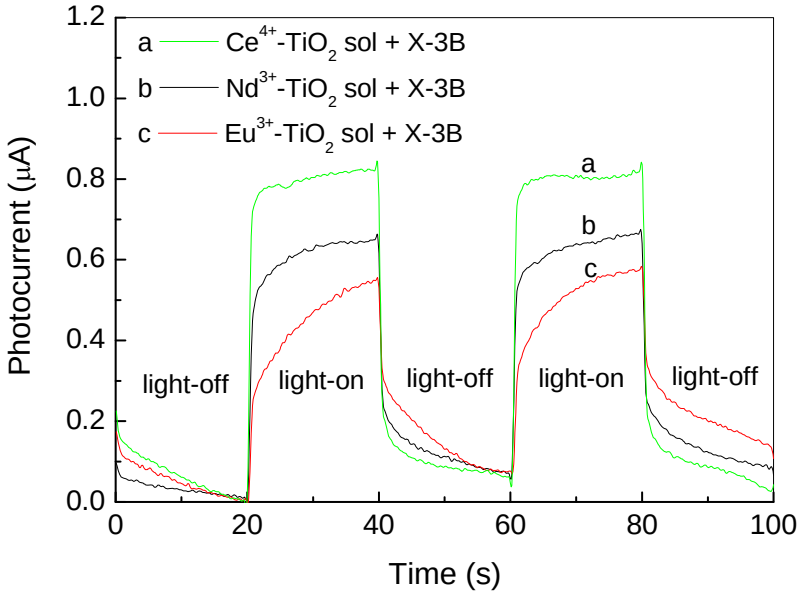
a Ce4+-TiO2 sol + X-3B
b Nd3+-TiO2 sol + X-3B
c Eu3+-TiO2 sol + X-3B
Photocurrent (μA)
Time (s)
light-off
light-on
light-off
light-on
light-off
a
b
c
0.0
0.2
0.4
0.6
0.8
1.0
1.2
0
20
40
60
80
100

Fig. 10.

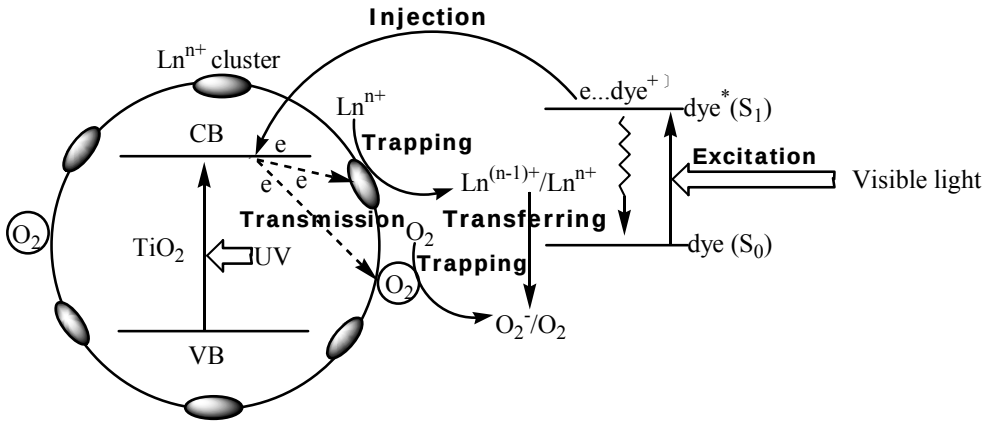
Injection
Ln^n+ cluster
Ln^n+
e...dye^+
dye*(S1)
CB
e
Trapping
Excitation
Visible light
e
e
Ln^(n-1)+/Ln^n+
Transmission
Transferring
O2
TiO2
UV
O2
Trapping
dye (S0)
O2
O2-/O2
VB

Fig. 11.

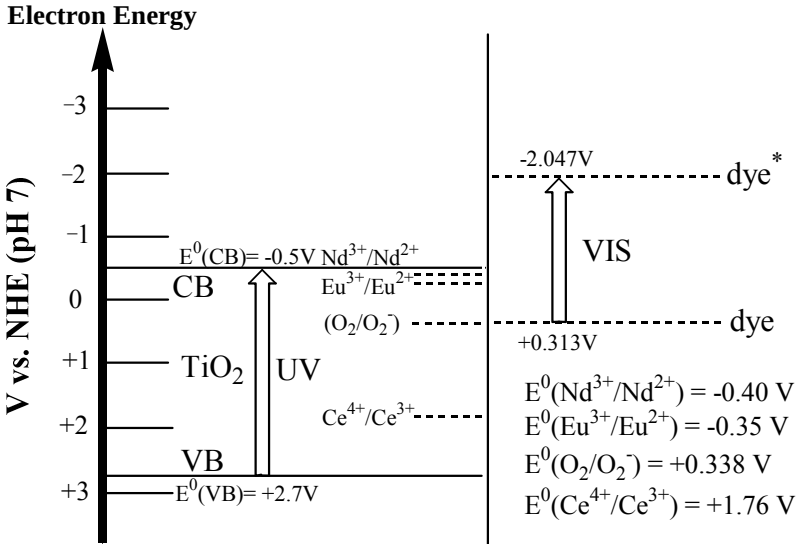
Electron Energy
V vs. NHE (pH 7)
−3
−2
−1
0
+1
+2
+3
E0(CB)= -0.5V Nd3+/Nd2+
CB
TiO2
UV
VB
E0(VB)= +2.7V
Eu3+/Eu2+
(O2/O2-)
Ce4+/Ce3+
-2.047V
dye*
VIS
dye
+0.313V
E0(Nd3+/Nd2+) = -0.40 V
E0(Eu3+/Eu2+) = -0.35 V
E0(O2/O2-) = +0.338 V
E0(Ce4+/Ce3+) = +1.76 V

Fig. 12.